JCTC Journal of Chemical Theory and Computation

Article

pubs.acs.org/JCTC

Modeling Molecular Systems at Extreme Pressure by an Extension of the Polarizable Continuum Model (PCM) Based on the Symmetry-Adapted Cluster-Configuration Interaction (SAC−CI) Method: Confined Electronic Excited States of Furan as a Test Case

Ryoichi Fukuda*[,†,‡] and Masahiro Ehara[†,‡]

[†]Institute for Molecular Science and Research Center for Computational Science, 38 Nishigo-naka, Myodaiji, Okazaki 444-8585, Japan

[‡]Elements Strategy Initiative for Catalysts and Batteries (ESICB), Kyoto University, Kyoto 615-8520, Japan

Roberto Cammi*

Dipartmento di Chimica, Università di Parma, Viale Parco Area delle Scienze 17/A, 43100 Parma, Italy

Supporting Information

ABSTRACT: Novel molecular photochemistry can be developed by combining high pressure and laser irradiation. For studying such high-pressure effects on the confined electronic ground and excited states, we extend the PCM (polarizable continuum model) SAC (symmetry-adapted cluster) and SAC−CI (SAC−configuration interaction) methods to the PCM-XP (extreme pressure) framework. By using the PCM-XP SAC/SAC−CI method, molecular systems in various electronic states can be confined by polarizable media in a smooth and flexible way. The PCM-XP SAC/SAC−CI method is applied to a furan (C_4H_4O) molecule in cyclohexane at high pressure (1−60 GPa). The relationship between the calculated free-energy and cavity volume can be approximately represented with the Murnaghan equation of state. The excitation energies of furan in cyclohexane show blueshifts with increasing pressure, and the extents of the blueshifts significantly depend on the character of the excitations. Particularly large confinement effects are found in the Rydberg states. The energy ordering of the lowest Rydberg and valence states alters under high-pressure. The pressure effects on the electronic structure may be classified into two contributions: a confinement of the molecular orbital and a suppression of the mixing between the valence and Rydberg configurations. The valence or Rydberg character in an excited state is, therefore, enhanced under high pressure.

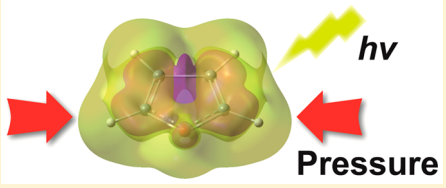

1. INTRODUCTION

A quantum mechanical (QM) model for studying molecular systems within a medium at high pressure regime was proposed by Cammi and his co-workers.[1,2] The model, which is called PCM-XP (extreme pressure), is based on the polarizable continuum model (PCM) developed for studying molecular systems in solution.[3,4] The PCM-XP considers the high-pressure effect from the medium by the electrostatic and Pauli repulsion interactions between the continuously distributing solvents and the QM solute that is enclosed by a molecularly shaped cavity. The PCM-XP provided the accurate vibrational properties of molecules under high pressure at the single molecule level.[2,5] The PCM-XP would have the potential ability for understanding and predicting the high-pressure chemical phenomena from a quantum-chemical point of view.

By combining the high pressure and electronic transitions, it is possible to pioneer novel and rich molecular chemistry. It has been proposed that the combined use of high pressure and laser irradiation can regulate chemical reaction mechanisms and control the selectivity of reaction products.[6−8] Upon photochemistry at high pressure, the molecular geometries are constrained by the high density of media. Moreover, the electronic structure of reacting molecules would be modified by the effect of pressure. Quantum chemical methods are necessary for studying the high-pressure chemical phenomena that involve the quantum confinement effects on several electronic states. However, few computational methods are available on the confinement effects for electronically excited molecules with using quantum chemical models.[9,10] The purpose of this article is to present a new useful methodology for such research purposes, by combining a well-established quantum chemical method for excited states with the PCM-XP model, and by which systems in various electronic states can be confined in a smooth and flexible way.

The symmetry-adapted cluster (SAC) and SAC-configuration interaction (SAC−CI) methods have already been combined with the PCM for studying electronic excitations of

Received: December 19, 2014
Published: April 14, 2015

DOI: 10.1021/ct5011517
J. Chem. Theory Comput. 2015, 11, 2063−2076

molecular systems in solution.[11] The SAC−CI is a well-established method for studying excited-state chemistry, and the PCM SAC/SAC−CI has been applied successfully to spectroscopy and photochemistry of various solvated systems. In this study, we extend the PCM SAC and PCM SAC−CI to the PCM-XP framework and develop the PCM-XP SAC and SAC−CI methods for considering the high-pressure effect on the ground and excited states at the correlated wave function level.

The new PCM-XP SAC/SAC−CI method was tested for studying the furan (C_4H_4O) molecule at high pressure (1−60 GPa) in a polarizable medium. The photochemistry of furan at high pressure has been reported by the crystalline state experiments.[12,13] At an isolated molecule level, the low-lying excited states of furan have been well studied theoretically.[14] Its low-lying excited states are characterized by the findings that the valence and several Rydberg excited states exist in the energy range of 1 eV. Moreover, a significant mixing of the valence and Rydberg characters are found in these states. It has been reported that the low-lying Rydberg states are responsible for photochemical bond cleavage of isolated furan molecules;[15] however, the Rydberg states would be destabilized in a condensed phase and not involved in the high-pressure photochemistry.[16] Therefore, it has been proposed that the photochemical reaction mechanism in the high-pressure crystalline furan is different from that of isolated molecule.[8,13]

Using the PCM-XP SAC/SAC−CI, we obtained the energetics of the furan molecule in the ground and excited states. The calculated free-energies are approximately represented with the Murnaghan equation of state[17] as a function of the cavity volume or the pressure. The excitation energies show blueshifts with increasing pressure, and larger shifts are found in the Rydberg states than in the valence states. As a result, the energy ordering of the lowest Rydberg and valence states alters under high pressure around 10−20 GPa. The present calculations show that the electronic structures of furan are significantly modified by the high-pressure effect. We found there are two types of the pressure effects on the electronic structure: a confinement of molecular orbital and a suppression of the mixing between the valence and Rydberg configurations. The latter is important for the excited states where the valence and Rydberg characters are mixed.

This article is organized as follows: first, we give an overview of the PCM-XP model and introduce the PCM-XP SAC/SAC−CI method in section 2. Section 3 describes the computational protocol of the molecular quantum chemistry under extreme pressure using the PCM-XP SAC/SAC−CI method. Section 4 gives the results and discussions for the test calculations of furan molecule under high pressure. Finally, section 5 presents the summary of this study.

2. THEORY

Within the PCM-XP model, the external medium is described both as a polarizable dielectric medium and as a uniform distribution of electrons, with the polarizable dielectric characterized by the bulk dielectric permittivity, and with the uniform distribution of electrons characterized by the bulk density of the valence electrons. The molecular solute is described at the QM level and occupies a void molecularly shaped cavity in the medium. To mimic the effects of pressure, the size of the cavity hosting the molecular solute is suitably shrunk with respect to the default cavity size used for PCM calculations in standard conditions of pressure.

2.1. Basic PCM-XP Energy Functional.

The target molecule that is interacting with a dense environment at high pressure is described by the nonlinear Schrödinger equation with the form

$$[H^0 + V_{\mathrm{int}}(\Psi_i)]\Psi_i = E_i\Psi_i \tag{1}$$

where H^0 is the Hamiltonian of the isolated molecule, and Ψ_i is the wave function of the solute for the i-th electronic state. The molecule-environment interaction operator denoted by $V_{\mathrm{int}}(\Psi_i)$ consists of two contributions:[1,2]

$$V_{\mathrm{int}}(\Psi_i) = V_e(\Psi_i) + V_r \tag{2}$$

Here, $V_e(\Psi_i)$ and V_r represent, respectively, the electrostatic and nonelectrostatic Pauli repulsion interactions between the solute and solvent. The solute−solvent dispersion interaction is not considered in this study.

The operator $V_e(\Psi_i)$ is represented in terms of a set of apparent polarization charges located at the cavity surface, and it may be written as

$$V_e(\Psi_i) = \mathbf{Q}(\Psi_i;\, \varepsilon)\cdot\mathbf{V} \tag{3}$$

where $\mathbf{Q}(\Psi_i;\varepsilon)$ is a vector collecting the set of polarization charges that represent the polarization of the solvent, $\mathbf{V}$ is a vector operator representing the electrostatic potential of the solute at the boundary of the cavity, and the dot represents an inner product. The solvent polarization charges $\mathbf{Q}(\Psi_i;\varepsilon)$ depend on the wave function of solute (Ψ_i) and on the dielectric permittivity of the solvent (ε). In general, the polarization charges are specific to the electronic state that we are interested in, via the wave function Ψ_i such as $\mathbf{Q}(\Psi_i;\varepsilon) = \langle\Psi_i|\mathbf{Q}(\varepsilon)|\Psi_i\rangle$; thus, this scheme is termed state-specific solvation. With the PCM-XP model, the ε value depends on a scaling factor (f) that is used to shrink the PCM cavity to consider the effect from the increase of pressure; the details are given in section 3. There are several definitions of the $\mathbf{Q}$ operator. Here, we refer to the most general variant, the integral equation formalism (IEF) PCM,[18−20] to which the model of Chipman[21] is closely related.[22]

The Pauli repulsion operator V_r of eq 2 can be written as

$$V_r(\mathbf{r}) = \rho(\mathbf{r})H(\mathbf{r}) \tag{4}$$

where $\rho(\mathbf{r}) = \sum_i^N \delta(\mathbf{r}-\mathbf{r}_i)$ is the electron density operator over the N electrons of the solute molecule, and $H(\mathbf{r})$ is a repulsive step barrier potential at the boundary of the cavity:

$$H(\mathbf{r}) = V_0\Theta(\mathbf{r}), \qquad \Theta(\mathbf{r}) = \begin{cases} 1 & \mathbf{r} \subseteq \mathbf{C}(\mathrm{cavity}) \\ 0 & \mathbf{r} \not\subset \mathbf{C}(\mathrm{cavity}) \end{cases} \tag{5}$$

where $\Theta(\mathbf{r})$ denotes a Heaviside step function located at the boundary of the cavity, and V_0 is the height of the potential barrier given by

$$V_0 = \gamma n_S^e \tag{6}$$

Here, γ is a semiempirical parameter, and n_S^e is the numeral density of the valence electron of the external medium. We are assuming that both γ and n_S^e parameters depend on the scaling factor f; the details are given in section 3.

The basic free-energy functional associated with the Schrödinger equation, eq 1, to be minimized in the QM procedure is given by

DOI: 10.1021/ct5011517
J. Chem. Theory Comput. 2015, 11, 2063−2076

$$G_{e-r} = \left\langle \Psi_i \middle| H^0 + \frac{1}{2}\mathbf{Q}(\Psi_i;\, \varepsilon)\cdot\mathbf{V} + V_r \middle| \Psi_i \right\rangle + V_{nn} \tag{7}$$

where V_{nn} is the nuclei−nuclei interaction contribution in the presence of the external medium. The energy functional G_{e-r} has the thermodynamic status of a free-energy for the whole system of the molecule and environment. The reference state for G_{e-r} is composed of the noninteracting electrons and nuclei of solute and the medium with a void molecular cavity at the chosen condition of temperature and pressure.

For a single determinant wave function of the solute, such as the Hartree−Fock wave function, with a basis set expansion of molecular orbitals (MOs), the free-energy functional G_{e-r} can be written in the following matrix form:

$$G_{e-r} = \left[tr\mathbf{Ph} + \frac{1}{2} tr\mathbf{PG}(\mathbf{P}) \right] + tr\mathbf{Ph}^e + \frac{1}{2} tr\mathbf{PX}^e(\mathbf{P}) + tr\mathbf{Ph}^r + V_{nn} \tag{8}$$

Here, the $\mathbf{P}$ matrix describes the one-electron distribution of solute in the given basis set. In eq 8, the first two terms in the square brackets correspond to the usual one ($\mathbf{h}$)- and two-electron ($\mathbf{G}(\mathbf{P})$) contributions to the energy of the isolated molecule. The matrices $\mathbf{h}^e$ and $\mathbf{X}^e(\mathbf{P})$ collect, respectively, one- and two-electron integrals describing the electrostatic interaction with the solvent. The matrix $\boldsymbol{h}^r$ collects the one-electron integrals that represent the Pauli repulsion operator V_r of eq 4. All of the matrix elements are the sum of integrals referring each to the representative point of a tessera of the cavity surface.

The explicit expression for the matrix elements of $\mathbf{h}^r$ with basis functions $\{\chi\}$ may be written as

$$h^r_{\mu\nu} = V_0\langle \chi_\mu | v_r | \chi_\nu \rangle \tag{9}$$

where v_r is a one-electron integral operator with kernel $v_r(\boldsymbol{r}) = \delta(\boldsymbol{r}-\boldsymbol{r}')\Theta(\boldsymbol{r})$. Using the Gauss divergence theorem, eq 9 can be reduced to

$$h^r_{\mu\nu} = V_0(S_{\mu\nu} - S^{in}_{\mu\nu}) \tag{10}$$

where $S_{\mu\nu}$ is an element of an overlap matrix, and $S^{in}_{\mu\nu}$ is given by

$$S^{in}_{\mu\nu} = \frac{1}{4\pi}\sum_k a_k \mathbf{E}_{\mu\nu}(\mathbf{s}_k)\cdot\mathbf{n}_k(\mathbf{s}_k) \tag{11}$$

with the summation running over the tesserae. The elements a_k, $\mathbf{E}_{\mu\nu}(\mathbf{s}_k)$, and $\mathbf{n}_k(\mathbf{s}_k)$, are, respectively, the area of the k-th tessera, a matrix element of the electric field integrals evaluated at the representative point $\mathbf{s}_k$, and the normal unit vector to the tessera at the same point. The free-energy functional of eq 8 subjected to the stationary conditions leads to the Fock matrix for the molecular solute:

$$F^{e-r}_{\mu\nu} = \frac{\partial G_{e-r}}{\partial P_{\mu\nu}} = (h_{\mu\nu} + h^e_{\mu\nu} + h^r_{\mu\nu}) + G_{\mu\nu}(\mathbf{P}) + X^e_{\mu\nu}(\mathbf{P}) \tag{12}$$

2.2. PCM-XP SAC and SAC−CI. The theoretical framework of the PCM-XP SAC and SAC−CI is similar to the usual PCM SAC and SAC−CI theories[11] except for the presence of the Pauli repulsion term at the one-electron operator level. In the PCM SAC theory for a closed-shell ground state, the energy and wave function are calculated with the following equation:

$$\langle \tilde{0}|S_K(H^{\mathrm{PCM}}_N - \Delta E^{\mathrm{PCM}}_{\mathrm{SAC}})|\Psi_{\mathrm{SAC}}\rangle = 0 \tag{13}$$

The SAC wave function is written as

$$|\Psi_{\mathrm{SAC}}\rangle = \exp\Big(\sum_I c_I S^\dagger_I\Big)|\tilde{0}\rangle \tag{14}$$

where $S^\dagger_I$ and c_I represent a symmetry-adapted excitation operator and its coefficient, respectively. We consider single and double electron excitations from a reference state $|\tilde{0}\rangle$ that is obtained by the PCM-XP Hartree−Fock equations. The correlation energy is written as

$$\Delta E^{\mathrm{PCM}}_{\mathrm{SAC}} = \langle \tilde{0}|H^{\mathrm{PCM}}_N|\Psi_{\mathrm{SAC}}\rangle \tag{15}$$

The PCM-XP SAC Hamiltonian includes the self-consistent charge and potential with respect to the SAC wave function:

$$H^{\mathrm{PCM}}_N = H^{\mathrm{HF}}_N + (\langle\Lambda|Q_N|\Psi_{\mathrm{SAC}}\rangle - \langle\Lambda'|\Psi_{\mathrm{SAC}}\rangle\langle\tilde{0}|Q_N|\Psi_{\mathrm{SAC}}\rangle)\cdot V_N \tag{16}$$

where Q_N and V_N denote the normal ordered form of the charge operator and the electronic potential operator, respectively, given in eq 3. The left vectors of the SAC equations are written as

$$\langle\Lambda'| = \langle\tilde{0}|\sum_K z^{\mathrm{SAC}}_K S_K \tag{17}$$

and $\langle\Lambda| = \langle\tilde{0}| + \langle\Lambda'|$, where S_K and z^{SAC}_K are the de-excitation operator and corresponding amplitude, respectively. The PCM reaction field at the Hartree−Fock level is considered in H^{HF}_N. In the PCM-XP SAC theory, the Pauli repulsion operator is included in H^{HF}_N as the usual one-electron operators. In the viewpoint of practical computations, the Hartree−Fock reaction field is considered in the Fock operator; consequently, the PCM-XP SAC computation procedure is essentially the same as that of the usual PCM SAC, except for using the MOs and Fock operator obtained by the PCM-XP Hartree−Fock theory. The PCM-XP SAC free-energy is given by

$$\Delta G^{\mathrm{SAC}}_{e-r} = \Delta E^{\mathrm{PCM}}_{\mathrm{SAC}} + \frac{1}{2}\Delta Q_{\mathrm{SAC}}\cdot\Delta V_{\mathrm{SAC}} \tag{18}$$

where

$$\Delta Q_{\mathrm{SAC}} = \langle\Lambda|Q_N|\Psi_{\mathrm{SAC}}\rangle - \langle\Lambda'|\Psi_{\mathrm{SAC}}\rangle\langle\tilde{0}|Q_N|\Psi_{\mathrm{SAC}}\rangle \tag{19}$$

and

$$\Delta V_{\mathrm{SAC}} = \langle\Lambda|V_N|\Psi_{\mathrm{SAC}}\rangle - \langle\Lambda'|\Psi_{\mathrm{SAC}}\rangle\langle\tilde{0}|V_N|\Psi_{\mathrm{SAC}}\rangle \tag{20}$$

The PCM SAC−CI secular equations for the p-th electronic state are written as

$$H^{\mathrm{PCM},p}_N|\Psi^p_{\mathrm{SAC\text{-}CI}}\rangle = \Delta E^{\mathrm{PCM},p}_{\mathrm{SAC\text{-}CI}}|\Psi^p_{\mathrm{SAC\text{-}CI}}\rangle \tag{21}$$

and

$$\langle\bar{\Psi}^p_{\mathrm{SAC\text{-}CI}}|H^{\mathrm{PCM},p}_N = \langle\bar{\Psi}^p_{\mathrm{SAC\text{-}CI}}|\Delta E^{\mathrm{PCM},p}_{\mathrm{SAC\text{-}CI}} \tag{22}$$

where $|\Psi^p_{\mathrm{SAC-CI}}\rangle$ and $\langle\bar{\Psi}^p_{\mathrm{SAC-CI}}|$ are the right and left SAC−CI vectors, respectively, with the energy of $\Delta E^{\mathrm{PCM},p}_{\mathrm{SAC-CI}}$. The vectors are written as

$$|\Psi^p_{\mathrm{SAC\text{-}CI}}\rangle = \sum_M d^p_M R^\dagger_M|\Psi_{\mathrm{SAC}}\rangle \tag{23}$$

and

$$\langle\bar{\Psi}^p_{\mathrm{SAC\text{-}CI}}| = \sum_M \bar{d}^p_M\langle\tilde{0}|R_M \tag{24}$$

DOI: 10.1021/ct5011517
J. Chem. Theory Comput. 2015, 11, 2063−2076

where $R_M^\dagger$ is the excitation operator with the coefficient d_M^p, and $\overline{d}_M^p$ is the coefficient of the left vector for R_M. The state-specific PCM-XP SAC−CI Hamiltonian for the solute in the p-th electronic state is

$$H_N^{\mathrm{PCM},p} = H_N^{\mathrm{HF}} + \Delta Q_{\mathrm{SACCI}}^{p} \cdot V_N \tag{25}$$

where

$$\Delta Q_{\mathrm{SACCI}}^{p} = \langle \overline{\Psi}_{\mathrm{SAC\text{-}CI}}^{p} | Q_N | \Psi_{\mathrm{SAC\text{-}CI}}^{p} \rangle \tag{26}$$

is the polarization charge at the SAC−CI level. Again, the Pauli repulsion operator is included in H_N^{HF}; therefore, the PCM-XP SAC−CI computation procedure is the same as that of the usual PCM SAC−CI using the MOs and Fock operator obtained by the PCM-XP Hartree−Fock theory. The PCM-XP SAC−CI free-energy is given by

$$\Delta G_{e-r}^{\mathrm{SAC\text{-}CI},p} = \Delta E_{\mathrm{SAC\text{-}CI}}^{\mathrm{PCM},p} + \frac{1}{2}\Delta Q_{\mathrm{SACCI}}^{p} \cdot \Delta V_{\mathrm{SACCI}}^{p} \tag{27}$$

The PCM-XP SAC−CI equations are nonlinear and state-specific; therefore, an iterative procedure is necessary for every electronic state. The PCM-XP SAC−CI excitation energies are defined by the difference of the free-energies:

$$\Delta\Delta G_{e-r}^{\mathrm{SAC\text{-}CI},p} = \Delta G_{e-r}^{\mathrm{SAC\text{-}CI},p} - \Delta G_{e-r}^{\mathrm{SAC}} \tag{28}$$

2.3. Pressure. The calculation of the pressure is a crucial step of the PCM to model the molecular system at extreme pressures. Pressure is a macroscopic thermodynamic property that can be related to a single molecule calculation by a suitable choice of a statistical mechanical ensemble.[23,24] Within the PCM-XP model, a canonical ensemble leads to define the pressure p as the minus of the derivative of the basic free-energy functional given by eq 7 with respect to the volume of the cavity:

$$p = -\left(\frac{\partial G_{e-r}}{\partial V_c}\right) \tag{29}$$

where V_c is the volume of the cavity hosting the solute molecule.

An expression of pressure similar to eq 29 has been used for confined systems with spherical or ellipsoidal cavities.[10,25−28] The PCM uses a molecularly shaped cavity that is generated by a set of overlapping spheres. The volume of the cavity may be freely reduced by using a scaling factor, while its shape is retained. Therefore, the PCM-XP model can confine systems in a smooth and flexible way.[27] Another approach to the quantum definition of pressure has been proposed by Bader for molecular systems, where the pressure is determined as the quantum force exerted per area of the boundary surface.[29]

3. COMPUTATIONAL PROTOCOL

The PCM-XP calculations require the definition of the cavity volume V_c as a variable. Also, the physical parameters characterizing solute−solvent interaction, the dielectric permittivity of the medium, its numeral density, and the Pauli step barrier potential depend on the variation of the cavity volume.

3.1. Cavity Scaling Factor *f*. In the standard PCM, the cavity is built-up from a set of primary atomic spheres centered on the nuclei of constituting atoms, with radii R_i equal to the corresponding van der Waals radii (R_{vdW}) times a scaling factor f, namely

$$R_i = R_{vdW} f \tag{30}$$

In the usual PCM calculations at the standard condition of pressure, the scaling factor is fixed at $f = 1.2$. In the PCM-XP, the cavity volume is varied by using a lower value of $f < 1.2$ that reduces the cavity volume V_c via decreasing the spheres' radii R_i and increases the pressure.

3.2. Dielectric Permittivity and the Repulsive Step Potential. The dielectric permittivity ε and numeral density of the external media are assumed as functions of the cavity scaling factor f. For a given choice of the scaling factor $f < 1.2$, we define the ratio s/f_0 between the volume of the cavity $V_c(f)$ at the given f and the reference cavity volume $V_c(f_0)$ with the reference scale factor $f_0 = 1.2$:

$$\frac{s}{f_0} = \left(\frac{V_c(f)}{V_c(f_0)}\right)^{1/3} \tag{31}$$

thus, $s/f_0 < 1$ for $f < 1.2$. The dielectric permittivity $\varepsilon(s/f_0)$ is given by the function of s/f_0 as

$$\varepsilon(s/f_0) = 1 + (\varepsilon_0 - 1)(f_0/s)^3 \tag{32}$$

where ε_0 is the dielectric permittivity of the medium at the standard pressure condition. This formula is derived from the Onsager equation for dielectric permittivity[30,31] by assuming a nonpolar medium whose polarizability is independent of the pressure. The factor $(f_0/s)^3$accounts for the increase of the numeral density of the medium; thus, eq 32 represents the linear relationship between $\varepsilon - 1$ and the increase of the numeral density of the medium. The density of the external medium $\rho_S(\eta;s/f_0)$ is given by

$$\rho_S(\eta;\, s/f_0) = \rho_S^0 (f_0/s)^{\eta+3} \tag{33}$$

where ρ_S^0 is the solvent density of the medium at the standard pressure condition. A semiempirical parameter η gauges the hardness of the Pauli repulsion barrier. The higher η value makes the Pauli repulsion barrier harder. The values $\eta = 3$ and 6 have been used on the basis of the comparison with the equation of state for $p-V$ of several solvents.[1,2,5]

In the PCM-XP, the barrier potential V_0 is represented by

$$V_0(\eta;\, s/f_0) = \gamma_0 N_S^e \frac{\rho_S(\eta;\, s/f_0)}{M_S^e} \tag{34}$$

where γ_0 is constant ($\gamma_0 = 4\pi/0.7E_h a_0^3$); M_S^e and N_S^e are, respectively, the molecular weight and the number of valence electrons of the solvent molecule.

Upon the practical computations of the PCM-XP, we will specify the solvent medium and give the scaling parameter f and gauge parameter η. The dielectric permittivity and density for a specified medium is calculated by eqs 32 and 33. The number of valence electrons and the molar weight of the solvent are uniquely defined.

3.3. Calculation of the Pressure. The pressure is associated with the cavity scaling factor f. The value $p(f)$ is evaluated by the finite difference method:

$$p(f) = -\left(\frac{G_{e-r}(f + \Delta f) - G_{e-r}(f)}{V_c(f + \Delta f) - V_c(f)}\right) \tag{35}$$

where $G_{e-r}(f)$ and $G_{e-r}(f+\Delta f)$ are the free-energy with the scaling factor f and $f+\Delta f$, respectively, and the cavity volumes

DOI: 10.1021/ct5011517
J. Chem. Theory Comput. 2015, 11, 2063−2076

Table 1. Excitation Energies (EE in eV), Electric Dipole Moment (μ in Debye), and Electronic Spatial Extent ($\langle r^2 \rangle$ in Å^2) for the Ground and Low-Lying Excited States of Furan in Vacuum and in Cyclohexane Solution at the Standard Condition of Pressure

	1-Ryd basis						2-Ryd basis						
	vacuum			in cyclohexane			vacuum			in cyclohexane			exp.[a]
state (nature)	EE (eV)	μ (D)[b]	$\langle r^2 \rangle$ (Å^2)	EE (eV)	μ (D)	$\langle r^2 \rangle$ (Å^2)	EE (eV)	μ (D)	$\langle r^2 \rangle$ (Å^2)	EE (eV)	μ (D)	$\langle r^2 \rangle$ (Å^2)	EE (eV)
X^1A_1 (GS[c])		−0.69	82.7		−0.77	82.7		−0.75	82.7		−0.85	82.7	
1^1A_2 (3s R[d])	5.90	0.81	96.6	5.83	1.12	98.2	5.91	0.81	96.4	5.84	1.10	98.1	5.91
1^1B_1 (3p R)	6.41	0.20	102.2	6.29	0.04	105.6	6.42	0.32	101.9	6.31	0.19	105.7	6.47
1^1B_2 (π^* V[e])	6.48	−3.45	92.3	6.40	−3.77	95.0	6.41	−3.27	90.5	6.35	−3.87	94.2	6.04
2^1A_2 (3p R)	6.57	1.26	103.7	6.40	0.04	107.3	6.59	1.25	103.6	6.42	0.02	107.8	6.61
2^1B_2 (3p R)	6.88	5.75	94.4	6.81	6.47	94.4	6.79	5.29	98.0	6.70	6.38	96.5	6.75

[a]Experimental values in gas phase taken from refs 40−44 and references therein. [b]We put the oxygen atom on the +z direction. [c]Ground state. [d]Rydberg state. [e]Valence excited state.

are $V_c(f)$ and $V_c(f+\Delta f)$. $\Delta f = \pm(0.001-0.002)$, is reasonable value for the finite difference.

When the pressure is expressed in GPa = 10^9 Jm^{-3}, eq 35 is

$$p(f)[\mathrm{GPa}] = -\frac{[G_{e-r}(f+\Delta f) - G_{e-r}(f)][\mathrm{kJ/mol}]}{[V_c(f+\Delta f) - V_c(f)][\mathrm{m}^3]} \times \frac{10^{-6}}{N_A} \cong -\frac{[G_{e-r}(f+\Delta f) - G_{e-r}(f)][\mathrm{E_h}]}{[V_c(f+\Delta f) - V_c(f)][\mathrm{Å}^3]} \times (4.3597 \times 10^3)[\mathrm{GPaÅ}^3/\mathrm{E_h}] \quad (36)$$

where N_A denotes Avogadro's constant.

4. TEST CALCULATIONS

4.1. Computational Details. The PCM-XP SAC/SAC−CI method was applied to the furan (C_4H_4O) molecule in cyclohexane. The ground-state molecular geometry in vacuum and in solution (without the Pauli repulsion) was optimized by the SAC and PCM SAC methods with the cc-pVDZ basis sets.[32] The effect of Pauli repulsion for the molecular geometry was estimated at the Hartree−Fock level. The molecular geometry was optimized by the PCM-XP Hartree−Fock method[2] for a given scaling factor f, and we obtained the f-dependent corrections for the geometrical parameters. For example, at $f = 0.90$, the decreases in the bond lengths are 0.015 Å for C═C, 0.007 Å for C−C, and 0.010 Å for C−O. For the PCM-XP SAC/SAC−CI calculations, the PCM SAC geometry was revised using these f-dependent corrections.

The cc-pVDZ sets with 1s1p1d Rydberg basis functions[33] (for $n = 3$: n denotes the principal quantum number) on C and O atoms were used for the energy calculations. To study the basis set dependences, the calculations with double Rydberg basis were performed for several cases. The Rydberg basis functions were split into two as $\alpha_1 = 1.9\alpha$ and $\alpha_2 = 0.75\alpha$, where α denotes the exponent of the original Gaussian basis function. Hereafter, the single Rydberg and double Rydberg basis sets denote 1-Ryd and 2-Ryd, respectively. For convenience of the computational program, the Cartesian form of the d-type basis functions (the so-called 6d basis) was employed.

For the SAC/SAC−CI calculations, 1s electrons of C and O atoms were treated as the frozen core, and the perturbation selection[34] was not used. The electric dipole moment and electronic spatial extent were calculated by using the unrelaxed SAC/SAC−CI density matrices where contributions from the coupled perturbed Hartree−Fock equations were neglected.[35] The calculations were performed by using the direct SAC−CI method[36] combined with the PCM SAC−CI and PCM-XP programs developed in Gaussian 09.[37]

The molecular cavity was generated using the scaled van der Waals surface with Bondi atomic radii.[38] No additional spheres were created to smooth the surface. Unlike previous PCM-XP calculations, we did not use the SES (solvent excluding surface) cavity because we encountered numerical instability upon the finite difference of eq 35. We used a simpler van der Waals surface with fine tesserae with an average arear of 0.10 Å^2. We chose cyclohexane as the external medium: $\varepsilon_0 = 2.0165$, $\rho_S^0 = 0.780$ g/mL, $M_S^e = 84.0$, and $N_S^e = 36$. We used $\eta = 3$ and $\eta = 6$ as the gauge parameters of the solvent density in eq 33. We found some discontinuousness of the cavity volume and the number of tesserae with respect to the continuous variation of the scaling factor f because the scaling is defined for atomic radii and not for the molecular cavity itself. Such discontinuous points were avoided when choosing f values. The IEF PCM[18−20] was used for evaluating the polarization apparent charges. The state-specific and equilibrium solvation scheme was used even for the vertical excitations in this study. In nonpolar solvents, the difference between the equilibrium and nonequilibrium schemes is small.[39]

4.2. Properties and Excitation Energies of Isolated and Solvated Furan. Table 1 shows the calculated excitation energies, electric dipole moment, and the electronic spatial extent ($\langle r^2 \rangle$: the expectation value of r^2 operator) of furan for its low-lying singlet states in vacuum and in cyclohexane solution at the standard condition of pressure where the solvent effect was considered by the PCM with the electrostatic term only. The results in vacuum agree with the previously reported SAC−CI results.[14] Use of the 2-Ryd basis slightly lowers the excitation energies of the 1^1B_2 and 2^1B_2 states due to the improvement of the valence description rather than the Rydberg description. The mixing of valence and Rydberg character is significant in these states. The effects of the 2-Ryd basis for other states are negligible.

Significant solvent effects around 0.1 eV are calculated even in nonpolar cyclohexane. Particularly, the solvent effect on the 2^1A_2 state is remarkable; its redshift reaches 0.17 eV. Such a large solvatochromic shift is attributed to the nature of this state. This state is a transition to the $3p_z$ Rydberg orbital; the molecule has the dipole moment in this direction. Con-

DOI: 10.1021/ct5011517
J. Chem. Theory Comput. 2015, 11, 2063−2076

Table 2. Calculated Pressure (p in GPa) for the Ground-State Furan in Cyclohexane at the Hartree−Fock (HF) and SAC Level with Respect to the Scaling Factor f for the Gauge Parameter η = 6 and 3[a]

			η = 6						η = 3		
					p (GPa)					p (GPa)	
f	s/f_0	ε	V_c (Å^3)	ρ_s (g/mL)	HF[b]	SAC[b]	HF[c]	SAC[c]	ρ_s (g/mL)	HF[b]	SAC[b]
1.200	1.000	2.0165	96.075	0.7800	0.7	0.7	0.9	0.9	0.7800	0.9	0.9
1.170	0.982	2.0718	91.116	0.9144	1.8	1.9	1.6	1.7	0.8672	1.4	1.5
1.108	0.946	2.2009	81.320	1.2863	3.2	3.3	3.2	3.3	1.0887	2.2	2.3
1.078	0.928	2.2717	76.793	1.5274	4.7	4.8	4.7	4.8	1.2209	3.0	3.1
1.060	0.917	2.3176	74.119	1.6988	5.7	5.9	5.8	5.9	1.3106	3.6	3.7
1.040	0.905	2.3712	71.223	1.9145	7.3	7.4	7.3	7.4	1.4193	4.4	4.5
1.018	0.892	2.4331	68.147	2.1857	10.6	10.7	10.6	10.7	1.5503	6.2	6.3
0.980	0.874	2.5240	64.082	2.6286	14.7	14.8	14.7	14.8	1.7532	8.1	8.2
0.958	0.855	2.6258	60.069	3.1914	21.1	21.2	21.0	21.2	1.9953	10.9	11.0
0.918	0.830	2.7800	54.864	4.1885	36.8	36.0	36.5	36.6	2.3919	17.6	17.7
0.900	0.818	2.8585	52.549	4.7669	44.4	44.4	43.9	44.1	2.6073	20.4	20.4
0.888	0.811	2.9090	51.158	5.1664	52.6	52.5	52.0	52.1	2.7510	23.6	23.7
0.880	0.805	2.9459	50.187	5.4721	60.2	60.0	59.5	59.5	2.8585	26.7	26.8
0.870	0.799	2.9933	48.994	5.8816	72.1	72.0	71.3	71.4	2.9994	31.6	31.7

[a]The cavity volume (V_c in Å^3), the dielectric permittivity (ε), and the solvent density (ρ_s in g/mL) are also shown. [b]1-Ryd basis. [c]2-Ryd basis.

sequently, the solute−solvent electrostatic interaction is particularly important in this state. Indeed the calculated dipole moments of this state in vacuum and in solution are quite different.

4.3. Ground State Energy and Pressure. The electron correlation gives only a small effect on the pressure. The calculated pressure values (p) with the PCM-XP Hartree−Fock and SAC methods are shown in Table 2 for the ground-state furan in cyclohexane. The scaling factor f = 1.20−0.87 spans the range of pressure 1−70 GPa with η = 6 and 1−30 GPa with η = 3. The electron correlation effects on the pressure are about 0.1 GPa and basically positive (pressure is increased by the correlation), but the effects depend on the basis set a little particularly at the very high pressure region. Using the 1-Ryd basis, the correlation effect on the pressure is negative (pressure is decreased by the correlation) for p > 50 GPa. Such decreasing effects are not obtained using the 2-Ryd basis. The calculated pressure at the SAC level using the 1-Ryd basis with respect to the cavity volume is shown in Figure 1.

Next, we intended to obtain an approximate relationship between the calculated pressure and the corresponding cavity volume. Here, we used the Murnaghan equation of state,[17] where B_0 and B' denote the bulk modulus and its derivative with respective to pressure, respectively.

$$p = \frac{B_0}{B'}\left[\left(\frac{V_c^0}{V_c}\right)^{B'} - 1\right] \tag{37}$$

According to the relationship in eq 20, we obtained the expression of free-energy as a function of the cavity volume by integrating eq 37 for $B' \neq 1$:

$$G_{e-r}(V_c) = G_{e-r}(V_c^0) + \frac{B_0 V_c}{B'}\left[\frac{1}{B'-1}\left(\frac{V_c^0}{V_c}\right)^{B'} + 1\right] - \frac{B_0 V_c^0}{B'-1} \tag{38}$$

The parameters B_0 and B' were obtained by the least-squares fitting of our computational results to eq 38 rather than eq 37

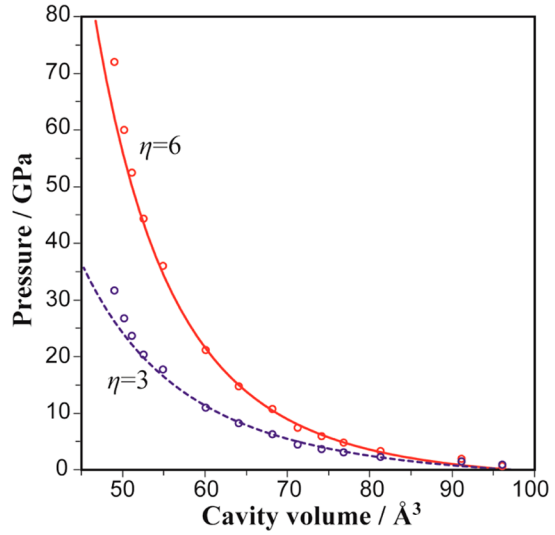

Figure 1. Calculated pressure at the SAC level using the 1-Ryd basis as a function of the cavity volume for η = 6 and η = 3. The solid and broken lines represent the Murnaghan equation of state (eq 37) with the corresponding fitting parameters.

because we can calculate the free-energy more precisely than the pressure. The obtained parameters for the ground states (X^1A_1 state) are shown in Table 3, and the V_c−p relationship of eq 37 is illustrated in Figure 1 with the solid and broken lines.

The PCM-XP results are represented well by the Murnaghan equation of state, although the deviations are relatively large for the smaller cavity volume. The electron correlation effects on the fitting parameters B_0 and B' are small. The η = 6 results give larger B_0 and B' values than the η = 3 results. We could not find the experimental values of the bulk modulus for crystalline furan at a high-pressure phase; however, these values are reasonable in comparison with those of other organic molecular crystals.[45,46] At high pressure, B_0 = 8 GPa and B' = 6.5 were proposed for benzene,[47] and B_0 = 10−23 and B' = 5−14.5 were proposed for cyclohexane.[48] On the basis of these values, the η = 6 results, which give B_0 = 11.5 GPa and B' = 4.9, seem to be

DOI: 10.1021/ct5011517
J. Chem. Theory Comput. 2015, 11, 2063−2076

Table 3. Bulk Modulus (B_0 in GPa) and Its Derivative with Respective to the Pressure (B') for Fitting the Murnaghan Equation of State to Our Calculated Results

state	B_0 (GPa)	B'
	η = 3, 1-Ryd Basis	
X^1A_1 (HF)	7.847	3.810
X^1A_1 (SAC)	8.981	3.623
1^1B_2	14.169	2.676
1^1A_2	21.581	1.717
1^1B_1	20.927	1.759
2^1A_2	20.055	1.883
2^1B_2	19.444	1.982
	η = 6, 1-Ryd Basis	
X^1A_1 (HF)	10.725	5.000
X^1A_1 (SAC)	11.510	4.914
1^1B_2	17.831	3.975
1^1A_2	31.128	3.219
1^1B_1	30.997	3.260
2^1A_2	31.477	3.160
2^1B_2	29.036	3.459
	η = 6, 2-Ryd basis	
X^1A_1 (HF)	10.725	4.990
X^1A_1 (SAC)	11.771	4.843
1^1B_2	18.224	3.939
1^1A_2	31.085	3.202
1^1B_1	30.910	3.248
2^1A_2	30.387	3.303
2^1B_2	29.123	3.427

more realistic than the η = 3 results for the present case of furan in cyclohexane.

We found that the total free-energy of the ground state can be approximated well by eq 38 as a function of V_c. The total free-energies of the ground-state SAC calculation with the 1-Ryd basis are plotted in Figure 2 against the cavity volume and the corresponding pressure for η = 3 (upper panels) and η = 6 (lower panels). The energy values are given in the Supporting Information. The total free-energy decreases with shrinking of the molecular cavity. The $G_{e-r} - V_c$ curves by eq 38 are also shown in the left panels of Figure 2 as solid and broken lines. The obtained relationship between the total free-energy and cavity volume depend on the choice of η to a certain degree. The use of larger η enhances the confinement effect on the energy.

The total free-energy in the ground state almost linearly depends on the pressure both for η = 3 and η = 6. The pressure dependence of the total free-energy is given in the right panels of Figure 2. The system is destabilized with increasing pressure. With regard to the pressure dependence of the free-energy, the η = 3 and η = 6 results give similar $G_{e-r}-p$ relationships. The use of smaller η enhances the pressure effect on the energy. Using eqs 37 and 38, the expression of free-energy as a function of the pressure is obtained as follows:

$$G_{e-r}(p) = G_{e-r}(V_c^0) + \frac{B_0 V_c^0}{B'}\left[\frac{1}{B'-1}\left(\frac{\tilde{B}'}{\tilde{B}_0}p + 1\right)^{(B'-1)/\tilde{B}'} + \left(\frac{\tilde{B}'}{\tilde{B}_0}p + 1\right)^{-1/\tilde{B}'}\right] - \frac{B_0 V_c^0}{B'-1} \quad (39)$$

where $\tilde{B}_0$ and $\tilde{B}'$ are the parameters obtained by the ground state calculations, while B_0 and B' are those for the target electronic state of $G_{e-r}(p)$. The relationships of eq 39 are shown in Figure 2 as solid and broken lines for η = 3 and η = 6. In the high-pressure region, in other words, with smaller cavity volume, the PCM-XP results deviate from eq 39. This is because eq 37 is not a good approximation for the smaller cavity volume. Additionally, the finite difference of eq 36 may involve some amount of numerical errors. According to the power series expansion of eq 39 with respect to p, the first-order term is predominant for the obtained B_0 and B' values; thus, the obtained $G_{e-r}-p$ curves for the ground state are approximately linear.

In the present system with the PCM-XP model, the correlation energy decreases with shrinking of the molecular cavity. The correlation energies (ΔG_{e-r}) of the ground-state SAC calculation with the 1-Ryd basis are plotted in Figure 3 against the cavity volume and the pressure. The energy values are given in the Supporting Information. The correlation energies are little affected by the choice of the parameter η. By assuming the relationship of eq 38 between the correlation energy and cavity volume, we obtained, by using the 1-Ryd basis, B_0 = 1.308 GPa and B' = 1.064 for η = 6, and B_0 = 1.308 GPa and B' = 1.154 for η = 3. These approximated relationships of $\Delta G_{e-r}-V_c$ are shown in the left panel of Figure 3. The pressure dependence of correlation energy is also approximated by eq 39 with the above obtained parameters, and the obtained $\Delta G_{e-r}-p$ curves are shown in the right panel of Figure 3. In the high-pressure region, those $\Delta G_{e-r}-p$ curves deviate from the calculated results because of the limitation of the Murnaghan equation of state and the numerical error from the finite difference. We found a certain difference in the $\Delta G_{e-r}-p$ relationships between the η = 3 and η = 6 results. The use of smaller η enhances the pressure effect on the correlation energy.

For a detailed discussion about the correlation energy, we need to note that we did not use the optimized geometry at the PCM-XP SAC level. The electron correlation can be divided into dynamical and nondynamical correlations. The dynamical correlation seems to decrease with increasing pressure. The nondynamical correlation also depends on the geometry. The nondynamical correlation increases when the geometry is far from the equilibrium, and the bond-lengths tend to shorten in high pressure. Thus, it is better to use the PCM-XP SAC equilibrium geometries for more detailed discussions about the pressure-dependence of correlation energies. Indeed, we obtained a different trend of the pressure effect on the correlation energy when we neglect the geometry relaxation (using the geometry at the standard condition for all calculations).

The decrease in the correlation energy by shrinking the molecular cavity in this model study disagrees with the previous studies for a confined helium atom and H_2 molecule, in which the correlation energies increase with decreasing confinement volume.[24−26] We could not find the reason for this disagreement; the possible reasons are the difference of models, the accuracy of computations for the correlation energy, excluding the core−electron correlation, and the intrinsic difference between furan and helium or the H_2 molecule.

4.4. Excited States. The extents of the energy decrease with shrinking the molecular cavity depend on the electronic states. The calculated free-energies of the excited states with the 1-Ryd basis are plotted in Figure 2 against the cavity volume

DOI: 10.1021/ct5011517
J. Chem. Theory Comput. 2015, 11, 2063−2076

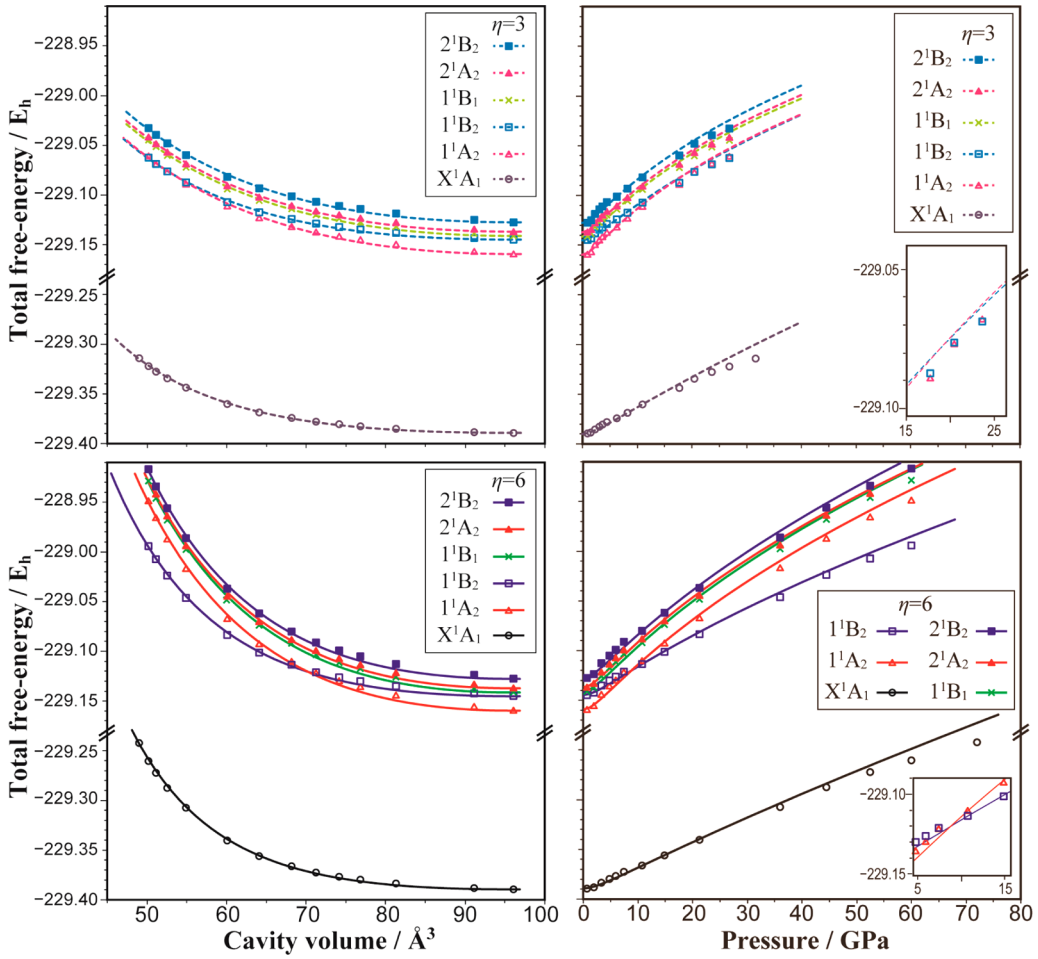

Figure 2. Total free-energies of PCM-XP SAC calculation for the variation of cavity volume and the corresponding pressure value with η = 3 (upper panels) and η = 6 (lower panels). The solid and broken lines represent the approximate curves obtained by eqs 38 and 39, respectively. The insertions in the right panels show the 1^1A_2 and 1^1B_2 states in 5−25 GPa where the energy ordering alters.

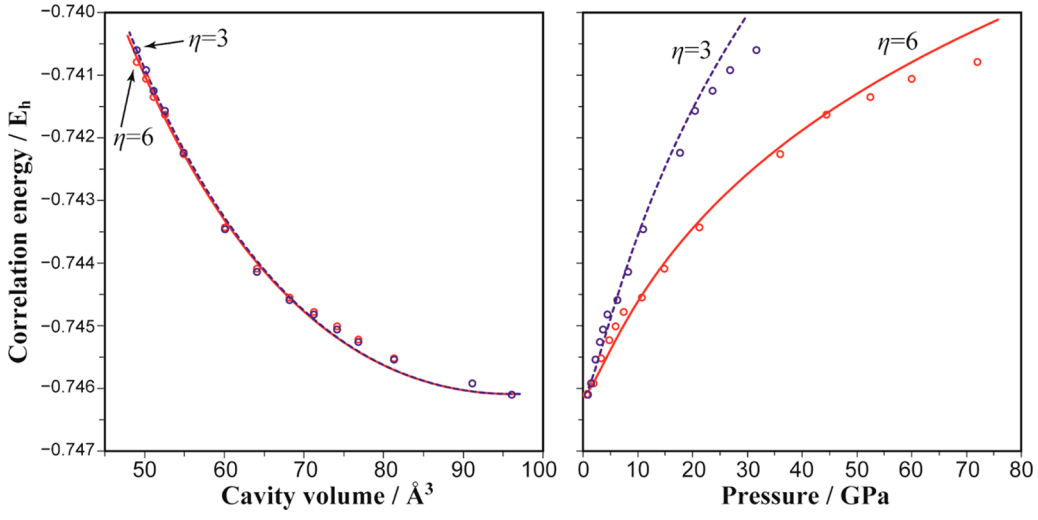

Figure 3. PCM-XP SAC correlation energies for the variation of cavity volume and the corresponding pressure value. The solid and broken lines represent the approximate curves obtained by eqs 38 and 39, respectively.

and the pressure. We suffered a convergence problem of the SAC−CI solutions with using small scaling factors; therefore, the results for f = 1.20−0.88 are shown. Using eq 38, the excited-state energies are expressed as a function of the cavity volume, and the optimal fitting parameters are shown in Table 3. The obtained $G_{e-r}-V_c$ curves are shown in Figure 2.

The values of the parameter B_0 for excited states are large in comparison with the ground state value. The B_0 obtained here for excited states is a parameter for the nonequilibrium vertical

DOI: 10.1021/ct5011517
J. Chem. Theory Comput. 2015, 11, 2063−2076

Table 4. Excitation Energies (in eV) for the Low-Lying Singlet States of Furan in Cyclohexane with Respect to the Scaling Factor f for the Gauge Parameter $\eta = 6$ and $\eta = 3$

	η = 6, 1-Ryd					η = 6, 2-Ryd					η = 3, 1-Ryd				
f	1^1B_2 (π^*)	1^1A_2 (3s)	1^1B_1 (3p)	2^1A_2 (3p)	2^1B_2 (3p)	1^1B_2 (π^*)	1^1A_2 (3s)	1^1B_1 (3p)	2^1A_2 (3p)	2^1B_2 (3p)	1^1B_2 (π^*)	1^1A_2 (3s)	1^1B_1 (3p)	2^1A_2 (3p)	2^1B_2 (3p)
1.200	6.66	6.26	6.76	6.88	7.14	6.56	6.27	6.77	6.89	7.06	6.66	6.26	6.76	6.88	7.14
1.170	6.69	6.33	6.83	6.95	7.20	6.59	6.33	6.84	6.95	7.12	6.68	6.31	6.80	6.92	7.17
1.108	6.76	6.52	7.02	7.13	7.37	6.65	6.52	7.02	7.13	7.28	6.73	6.41	6.90	7.01	7.26
1.078	6.79	6.64	7.14	7.25	7.48	6.69	6.64	7.14	7.25	7.39	6.75	6.47	6.96	7.06	7.31
1.060	6.82	6.73	7.22	7.33	7.56	6.71	6.72	7.22	7.33	7.47	6.77	6.51	6.99	7.09	7.34
1.040	6.85	6.83	7.33	7.44	7.66	6.74	6.82	7.33	7.43	7.57	6.79	6.55	7.04	7.14	7.38
1.018	6.88	6.96	7.46	7.57	7.79	6.78	6.95	7.46	7.56	7.70	6.81	6.61	7.09	7.18	7.43
0.980	6.93	7.17	7.67	7.78	7.99	6.84	7.16	7.66	7.77	7.90	6.85	6.69	7.16	7.26	7.50
0.958	6.99	7.44	7.94	8.05	8.26	6.91	7.42	7.93	8.03	8.16	6.89	6.78	7.25	7.34	7.58
0.918	7.11	7.91	8.42	8.53	8.74	7.03	7.88	8.40	8.51	8.63	6.98	6.94	7.40	7.48	7.72
0.900	7.17	8.17	8.70	8.81	9.02	7.11	8.15	8.68	8.78	8.91	7.02	7.02	7.47	7.56	7.80
0.888	7.21	8.35	8.88	8.99	9.20	7.15	8.32	8.86	8.97	9.09	7.05	7.07	7.52	7.61	7.85
0.880	7.24	8.48	9.03	NC[a]	9.35	7.19	8.45	9.00	9.11	9.23	7.07	7.11	7.56	7.64	7.88

[a]Solution did not converge.

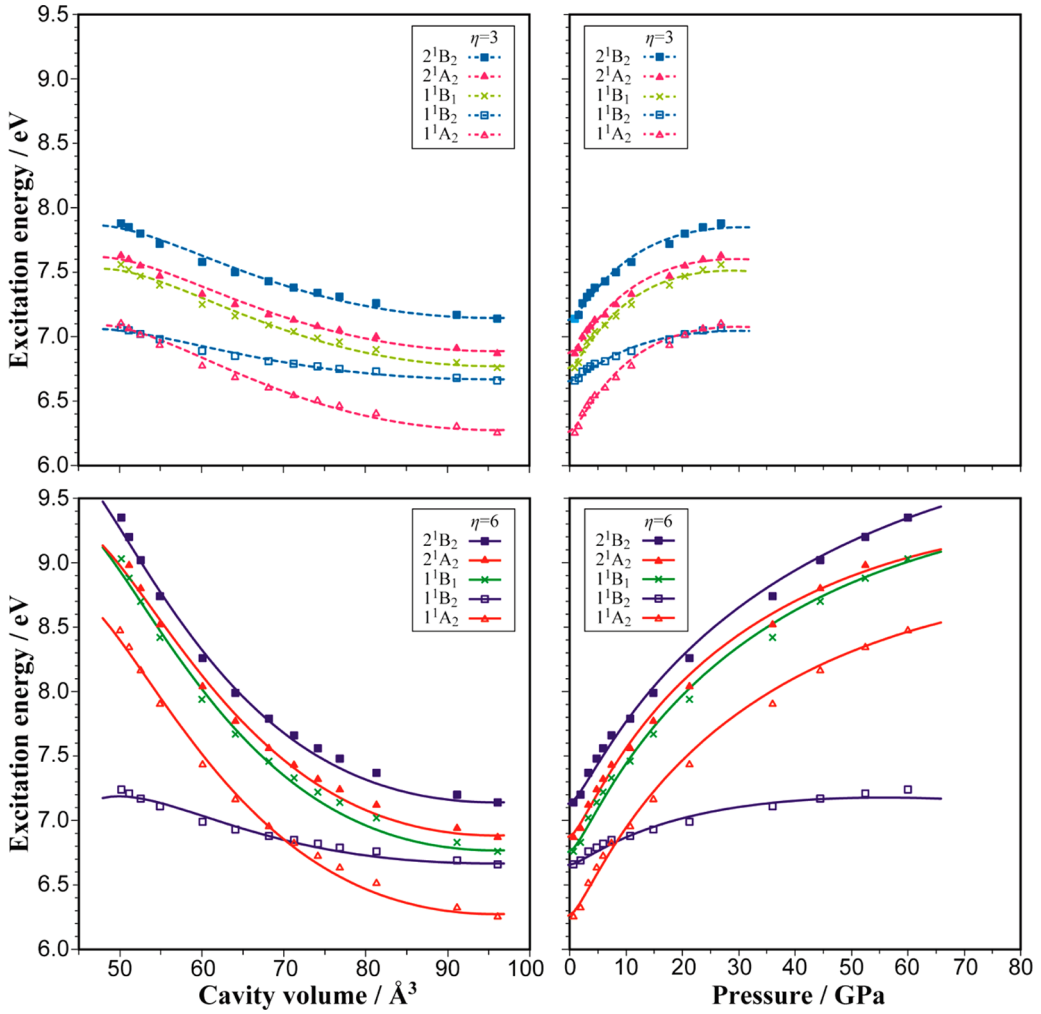

Figure 4. PCM-XP SAC−CI excitation energies of furan (1-Ryd basis) for the variation of cavity volume and the corresponding pressure value with $\eta = 3$ (upper panels) and $\eta = 6$ (lower panels). The approximate curves obtained by eqs 38 and 39 are also shown for $\eta = 3$ (broken line) and $\eta = 6$ (solid line).

excitations (the molecular geometry is not relaxed); therefore, it does not directly correspond to the observable bulk modulus. The larger B_0 parameter represents the fact that the free-energy variation is more sensitive to the variation of cavity volume. The B_0 values for the Rydberg states are larger than the valence excited state. Therefore, the free-energy variations with respect

DOI: 10.1021/ct5011517
J. Chem. Theory Comput. 2015, 11, 2063−2076

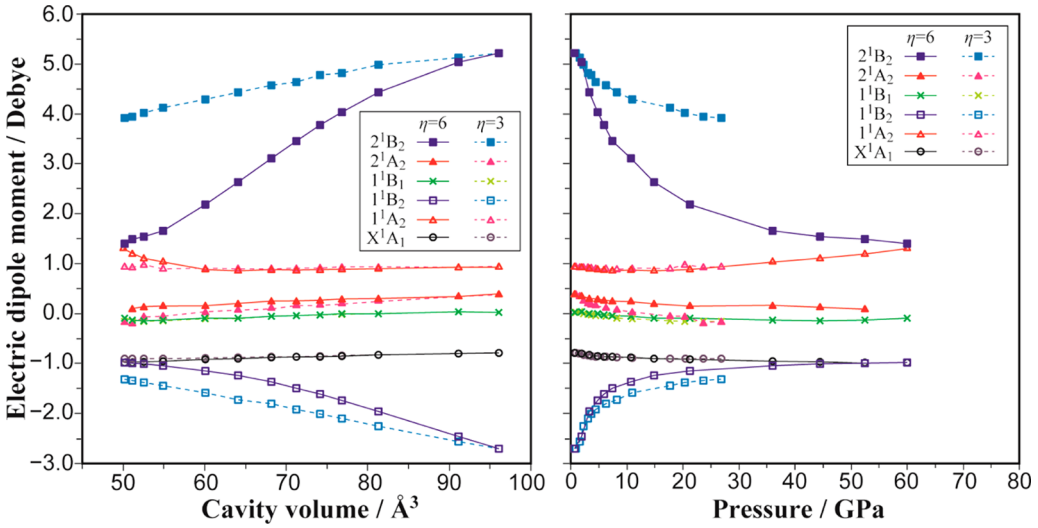

Figure 5. Calculated electric dipole moment of furan (1-Ryd basis) for the variation of cavity volume and the corresponding pressure value for $\eta = 3$ (broken line) and $\eta = 6$ (solid line).

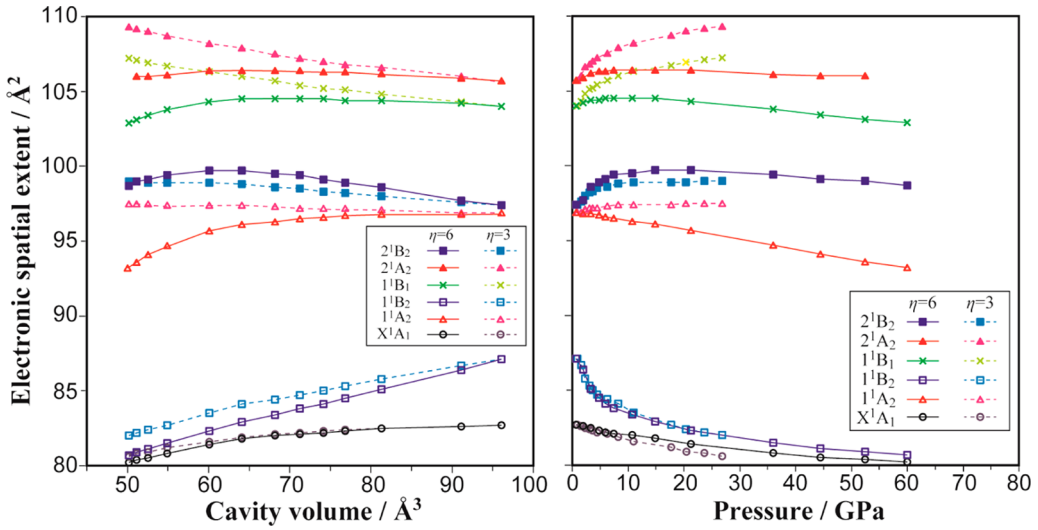

Figure 6. Calculated electronic spatial extent ($\langle r^2 \rangle$) of furan (1-Ryd basis) for the variation of cavity volume and the corresponding pressure value for $\eta = 3$ (broken line) and $\eta = 6$ (solid line).

to the shrinkage in the cavity volume are significantly different between the valence and Rydberg excited states. As a result of such a different behavior, the energy ordering alters between the valence 1^1B_2 and Rydberg 1^1A_2 states with shrinking of the molecular cavity (with increasing pressure).

In contrast to the ground state, the $G_{e-r}-p$ curves for the excited states have a certain curvature. The $G_{e-r}-p$ curves obtained by eq 39 for the excited states are also shown in Figure 2. The expression of free-energy as a function of the pressure is more complicated in the excited state than that in the ground state because the expression for excited state involves four parameters ($\tilde{B}_0$, $\tilde{B}'$, B_0, and B'), while the expression for the ground state involves only two parameters because $\tilde{B}_0 = B_0$ and $\tilde{B}' = B'$. That is to say, the pressure dependence of the excited-state free-energy is also associated with the variation of the ground-state free-energy through the pressure value.

4.5. Excitation Energies. The calculated excitation energies with the PCM-XP SAC−CI method are shown in Table 4. As in the case of isolated furan, use of the 2-Ryd basis slightly lowers the excitation energies of the 1^1B_2 and 2^1B_2 states; however, the amount of energy lowering is almost uniform with respect to the variation of the scaling factor. Therefore, the cavity-volume dependence of excitation energy does not significantly differ between the 1-Ryd and 2-Ryd basis results. Indeed, the optimal B_0 and B' parameters for the 1-Ryd and 2-Ryd results are very close. Figure 4 shows the variation of the excitation energies ($\Delta\Delta G_{e-r}$) with respect to the cavity volume and the corresponding pressure calculated with the 1-Ryd basis. The $\Delta\Delta G_{e-r}-V_c$ and $\Delta\Delta G_{e-r}-p$ curves in Figure 4 are obtained by eqs 38 and 39 by taking the difference between the ground and excited states.

The excitation energies increase with shrinking of the cavity volume for all of the calculated states, while the rate of increase in the excitation energy is significantly different between the valence and Rydberg excitations. The Rydberg excitation energies more steeply increase with shrinking of the cavity volume. As a result, the energy ordering of the lowest Rydberg (1^1A_2) and valence (1^1B_2) states alters at around 10 GPa ($\eta = 6$) or 20 GPa ($\eta = 3$). The lowest excitation is the 3s Rydberg

DOI: 10.1021/ct5011517
J. Chem. Theory Comput. 2015, 11, 2063−2076

(1^1A_2 state) in vacuum and under lower pressure conditions, whereas under higher pressure conditions, the lowest excitation is the valence π^* (1^1B_2 state).

From the present PCM-XP SAC−CI calculations, we found that the excitation energies of furan in cyclohexane show blueshifts with increasing pressure, and the extents of the blueshifts are significantly larger in Rydberg states than in the valence state. We could not find the experimental measurements that correspond to the presented model system; however, significant blueshifts of Rydberg state energy have been reported for benzene in condensed phase.[16] The blueshifts of the Rydberg state can be explained by the PCM-XP SAC−CI calculations. For the furan crystal, the lowest optical-absorption edge shows a redshift in the high pressure (1−40 GPa) UV−vis (ultraviolet−visible) absorption spectra.[13] This observation seems to contradict our computational results in which the lowest valence absorption shows a blueshift at high pressure. We think that the origins of the observed redshift in furan crystal are the electrostatic effect of surrounding furan molecules and the dispersion interaction between furan molecules. Furan is considered to be a more polar molecule than cyclohexane; therefore, surrounding furan molecules stabilize the valence excited state that has a large electric dipole moment. It is known that the dispersion interaction is an important origin of a redshift of π^* states, but it is not considered in this model.[49−53] A practical way to reproduce the experimental condition is to use a small cluster model combined with the PCM-XP.

4.6. Electronic Structure of Furan under High Pressures. The effects of pressure on the electronic structure are investigated in terms of the electric dipole moment and electronic spatial extent. The calculated electric dipole moment and the electronic spatial extent ($\langle r^2 \rangle$) with the 1-Ryd basis are plotted in Figures 5 and 6, respectively, against the cavity volume and the pressure. All of the calculated values are given in the Supporting Information. Except for the 1^1B_2 and 2^1B_2 states, the dipole moment does not change so significantly with respect to the variation of the cavity volume and the pressure. For the 1^1B_2 and 2^1B_2 states, the dipole moment correlated to the cavity volume and the pressure, and its η dependence is quite large in the 2^1B_2 state. In the 1^1B_2 and 2^1B_2 states, the absolute value of the dipole moment is diminished by the confinement effect. At 60 GPa, the dipole moment of the 2^1B_2 state is close to the value of the 1^1A_2 state, and the dipole moments of the 1^1B_2 and ground states are approximately equal in $p < 45$ GPa region. These findings indicate that the electron−hole charge separation induced by the electronic excitation is diminished by the confinement effect (pressure effect).

On the behavior of $\langle r^2 \rangle$ values, significant η dependence is observed for the Rydberg excitations. For $\eta = 6$, the $\langle r^2 \rangle$ values of the 1^1B_2, 2^1B_2, and 2^1A_2 states increase in $p < 10$ GPa region, and the values decrease in the $p > 10$ GPa region. For $\eta = 3$, however, the $\langle r^2 \rangle$ values of all of the Rydberg states do not decrease when the pressure is increased. In the ground and valence-excited 1^1B_2 states, the η dependence is small, and the $\langle r^2 \rangle$ values decrease with increasing pressure. The variation of the $\langle r^2 \rangle$ value of the 1^1B_2 state is significant in the $p < 10$ GPa region.

The above-mentioned behavior of the $\langle r^2 \rangle$ values can be explained with the two individual origins of the confinement effect (pressure effect). One is the condensation of the MOs originated in the confinement including the effects caused by the decreases in the bond lengths. The other is the variation of the mixing ratio of the valence and Rydberg characters in each electronic state. The first one is the origin of the constant decrease in the $\langle r^2 \rangle$ value of the ground state and those of the excited states for $p > 10$ GPa with $\eta = 6$. By using $\eta = 3$, however, such a confinement effect on the Rydberg orbitals would not be described well because the repulsive potential is too soft.

The behavior of $\langle r^2 \rangle$ in the region of $p < 10$ GPa is explained with the variation of the mixing ratio of the valence and Rydberg characters in an electronic state. In a small cavity (in high pressure), the energy of Rydberg orbitals is destabilized, and therefore, the configuration mixing of the valence and Rydberg is suppressed. Consequently, the valence character in the 1^1B_2 state is enhanced and its wave function becomes compact. In the Rydberg state, the Rydberg character is enhanced by the confinement effect, and their wave functions become more diffuse. Indeed, the SAC−CI coefficients of the excitation to Rydberg orbitals become large with shrinking of the molecular cavity.

The high-pressure photochemical reaction has been reported for the furan crystal at 3 GPa.[13] The study suggests that the reaction involves a preferential dissociation involving cleavage of the C−O bonds and that the valence π^* states, not the Rydberg state, must be relevant to the reaction. The present study supports the latter suggestion because the excitation energies of the Rydberg states are too high at high pressure. However, it has been found that the Rydberg states are responsible for photochemical C−O bond cleavage of the isolated furan molecule.[15] Thus, a different reaction mechanism needs to be supposed for the photochemical reaction of furan in solid phase. According to the present study, the electronic structure of the valence π^* state is significantly changed by the effect of high pressure. Therefore, the valence π^* state may alter its reactivity under an extreme pressure conditions.

5. SUMMARY

In this study, we develop the PCM-XP SAC and SAC−CI methods by extending the PCM SAC/SAC−CI to the PCM-XP framework for considering the high-pressure effects on the ground and excited states. The PCM-XP SAC/SAC−CI was applied to the furan molecule in cyclohexane at high pressure. Using the PCM-XP SAC/SAC−CI, we obtained reasonable relationships between the pressure and the free-energy of each electronic state. Between the calculated free-energy and cavity volume, we found the correlation that is approximately represented with the Murnaghan equation of state.

We found that the excitation energies of furan in cyclohexane show blueshifts with increasing pressure and that the extents of the blueshifts significantly depend on the character of the excitations. Larger confinement effects were found in the Rydberg states than in the valence state. Consequently, the energy ordering of the lowest Rydberg and valence states alters at around 10−20 GPa.

The effects of pressure on the electronic structure were investigated in terms of the electric dipole moment and the electronic spatial extent. We found that the pressure effects on the electronic structure may be classified into two contributions. One is a common confinement effect that reduces the spatial extent of electron density at the orbital level. The other is a suppression of the mixing between the valence and Rydberg configurations. As a result of the suppression of configuration mixing, the valence character or Rydberg character is enhanced

DOI: 10.1021/ct5011517
J. Chem. Theory Comput. 2015, 11, 2063−2076

under high pressure. A photochemical reactivity of molecules must be changed as a consequence of the pressure effects on the electronic structure.

The present method can confine systems in various electronic states by a smooth and flexible way. Additionally, we have already developed the analytical energy gradient of both PCM-XP and PCM SAC/SAC−CI. The implementation of the analytical energy gradient for the PCM-XP SAC/SAC−CI is straightforward. Therefore, the PCM-XP SAC/SAC−CI method is a favorable approach for studying high-pressure photochemistry.

APPENDIX

In this appendix, we discuss an interpolation method to estimate the excitation energies at a given value of pressure. In comparison with the $G_{e-r}-p$ curves, the $\Delta\Delta G_{e-r}-p$ curves estimated by eq 39 seem to reproduce well the actual computational results. This may be because of a cancellation of errors between the ground and excited states. Then, we have estimated the excitation energies at a given pressure by eq 39 and the parameters in Table 3, and the estimated excitation energies are compared with the actually computed results by the PCM-XP SAC−CI given in Table 4 for $\eta = 6$ and the 1-Ryd basis. Figure 7 shows the correlation between the estimated and actually calculated excitation energies. The excitation energies predicted by eq 39 accurately reproduced the actual PCM-XP SAC−CI results. The RMSD (root mean-square deviation) is 0.05 eV. A benefit of this interpolation method is as follows. As shown in the computational protocol, the pressure is not an external parameter in the PCM-XP model because the theory is based on the canonical ensemble (NVT ensemble). The pressure is obtained by the finite difference of eq 36 as the variation of total free-energy with respect to the cavity volume through the variation of the scaling factor. Namely, it is not easy to calculate the excitation energies at a given pressure value. Additionally, the accuracy of the finite difference requires serious attention. However, with using the interpolation method, we can estimate the excitation energies at an arbitrary pressure condition very easily once the parameters B_0 and B' have been determined.

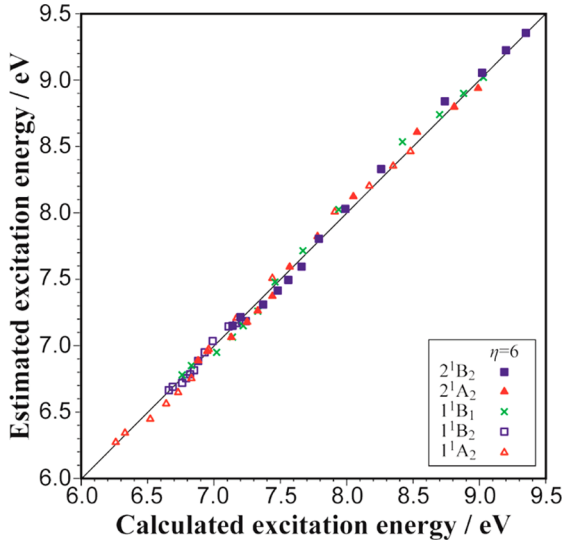

Figure 7. Correlation between the excitation energies of furan estimated by eq 39 and actually calculated excitation energies of furan with the 1-Ryd basis and $\eta = 6$.

ASSOCIATED CONTENT

Supporting Information

Energies in the ground state and the electric dipole moment and electronic spatial extent in all of the states. This material is available free of charge via the Internet at http://pubs.acs.org.

AUTHOR INFORMATION

Corresponding Authors

*(R.F.) E-mail: fukuda@ims.ac.jp.
*(R.C.) E-mail: roberto.cammi@unipr.it.

Notes

The authors declare no competing financial interest.

ACKNOWLEDGMENTS

This work was supported by a Grant-in-Aid for Scientific Research from the Japan Society for the Promotion of Science (JSPS), Japan; Nanotechnology Platform Program (Molecule and Material Synthesis) of the Ministry of Education Culture, Sports, Science and Technology (MEXT), Japan, and the MEXT program "Elements Strategy Initiative to Form Core Research Center". We thank Gaussian Inc. for collaboration. The computations were partially performed at the Research Center for Computational Science, Okazaki, Japan.

REFERENCES

(1) Cammi, R.; Verdolino, V.; Mennucci, B.; Tomasi, J. Towards the elaboration of a QM method to describe molecular solutes under the effect of a very high pressure. *Chem. Phys.* **2008**, *344*, 135−141.
(2) Cammi, R.; Cappelli, C.; Mennucci, B.; Tomasi, J. Calculation and analysis of the harmonic vibrational frequencies in molecules at extreme pressure: methodology and diborane as a test case. *J. Chem. Phys.* **2012**, *137*, 154112.
(3) Miertuš, S.; Scrocco, E.; Tomasi, J. Electrostatic interaction of a solute with a continuum. A direct utilization of ab initio molecular potentials for the prevision of solvent effects. *Chem. Phys.* **1981**, *55*, 117−129.
(4) Tomasi, J.; Mennucci, B.; Cammi, R. Quantum mechanical continuum solvation models. *Chem. Rev.* **2005**, *105*, 2999−3093.
(5) Pagliai, M.; Cardini, G.; Cammi, R. Vibrational frequencies of fullerenes C_{60} and C_{70} under pressure studied with a quantum chemical model including spatial confinement effects. *J. Phys. Chem. A* **2014**, *118*, 5098−5111.
(6) Ciabini, L.; Santoro, M.; Bini, R.; Schettino, V. High pressure photoinduced ring opening of benzene. *Phys. Rev. Lett.* **2002**, *88*, 085505.
(7) Citroni, M.; Ceppatelli, M.; Bini, R.; Schettino, V. Laser-induced selectivity for dimerization versus polymerization of butadiene under pressure. *Science* **2002**, *295*, 2058−2060.
(8) Bini, R. Laser-assisted high-pressure chemical reactions. *Acc. Chem. Res.* **2004**, *37*, 95−110.
(9) Borgoo, A.; Tozer, D. J.; Geerlings, P.; De Proft, F. Confinement effects on excitation energies and regioselectivity as probed by the Fukui function and the molecular electrostatic potential. *Phys. Chem. Chem. Phys.* **2009**, *11*, 2862−2868.
(10) Rossi, A. R.; Wang, Y.; Wiberg, K. B. Excited state and photochemistry of bicyclo[1.1.0]butane. *J. Chem. A* **2009**, *113*, 1686−1695.
(11) Cammi, R.; Fukuda, R.; Ehara, M.; Nakatsuji, H. Symmetry-adapted cluster and symmetry-adapted cluster-configuration interaction method in the polarizable continuum model: theory of the solvent effect on the electronic excitation of molecules in solution. *J. Chem. Phys.* **2010**, *133*, 024104.

DOI: 10.1021/ct5011517
J. Chem. Theory Comput. 2015, 11, 2063−2076

(12) Ceppatelli, M.; Santoro, M.; Bini, R.; Schettino, V. High pressure reactivity of solid furan probed by infrared and Raman spectroscopy. *J. Chem. Phys.* **2003**, *118*, 1499−1508.
(13) Santoro, M.; Ceppatelli, M.; Bini, R.; Schettino, V. High-pressure photochemistry of furan crystal. *J. Chem. Phys.* **2003**, *118*, 8321−8325.
(14) Wan, J.; Meller, J.; Hada, M.; Ehara, M.; Nakatsuji, H. Electronic excitation spectra of furan and pyrrole: revisited by the symmetry adapted cluster-configuration interaction method. *J. Chem. Phys.* **2000**, *113*, 7853−7866.
(15) Sorkhabi, O.; Qi, F.; Rizvi, A. H.; Suits, A. G. Ultraviolet photodissociation of furan probed by tunable synchrotron radiation. *J. Chem. Phys.* **1999**, *111*, 100−107.
(16) Scott, T. W.; Albrecht, A. C. A Rydberg transition in benzene in the condensed phase; two-photon fluorescence excitation studies. *J. Chem. Phys.* **1981**, *74*, 3807−3812.
(17) Murnaghan, F. D. The compressibility of media under extreme pressures. *Proc. Natl. Acad. Sci. U.S.A.* **1944**, *30*, 244−247.
(18) Cancès, E.; Mennucci, B.; Tomasi, J. A new integral equation formalism for the polarizable continuum model: theoretical background and applications to isotropic and anisotropic dielectrics. *J. Chem. Phys.* **1997**, *107*, 3032−3041.
(19) Mennucci, B.; Cancès, E.; Tomasi, J. Evaluation of solvent effects in isotropic and anisotropic dielectrics and in ionic solutions with a unified integral equation method: theoretical bases, computational implementation, and numerical applications. *J. Phys. Chem. B* **1997**, *101*, 10506−10517.
(20) Cancès, E.; Mennucci, B. New applications of integral equations methods for solvation continuum models: ionic solutions and liquid crystals. *J. Math. Chem.* **1998**, *23*, 309−326.
(21) Chipman, D. M. Reaction field treatment of the charge penetration. *J. Chem. Phys.* **2000**, *112*, 5558−5565.
(22) Cancès, E.; Mennucci, B. Comment on "Reaction field treatment of charge penetration". *J. Chem. Phys.* **2001**, *114*, 4744−4745.
(23) Brown, W. B. On the quantal virial equation for the pressure. *J. Chem. Phys.* **1958**, *28*, 522−523.
(24) Marc, G.; McMillan, W. G. The virial theorem. *Adv. Chem. Phys.* **1985**, *58*, 209−351.
(25) Gimarc, B. M. Correlation energy of the two-electron atom in a spherical potential box. *J. Chem. Phys.* **1967**, *47*, 5110−5115.
(26) Ludeña, E. V.; Gregori, M. Configuration interaction calculations for two-electron atoms in a spherical box. *J. Chem. Phys.* **1979**, *71*, 2235−2240.
(27) LeSar, R.; Herschbach, D. R. Electronic and vibrational properties of molecules at high pressures. Hydrogen molecule in a rigid spheroidal box. *J. Phys. Chem.* **1981**, *85*, 2798−2804.
(28) Sarsa, A.; Le Sech, C. Variational Monte Carlo method with dirichlet boundary conditions: application to the study of confined systems by impenetrable surfaces with different symmetries. *J. Chem. Theory Comput.* **2011**, *7*, 2786−2794.
(29) Bader, R. F. W. Confined atoms treated as open quantum systems. *Adv. Quantum Chem.* **2009**, *57*, 285−318.
(30) Böttcher, C. J. F. In *Theory of Electric Polarization*, 2nd ed.; Elsevier: Amsterdam, The Netherlands, 1973; Vol. *I*, Dielectrics in Static Fields.
(31) Wortmann, R.; Bishop, D. M. Effective polarizabilities and local field corrections for nonlinear optical experiments in condensed media. *J. Chem. Phys.* **1998**, *108*, 1001−1007.
(32) Dunning, T. H., Jr. Gaussian basis sets for use in correlated molecular calculations. I. The atoms boron through neon and hydrogen. *J. Chem. Phys.* **1989**, *90*, 1007−1023.
(33) Dunning, T. H., Jr.; Hay, P. J. In *Modern Theoretical Chemistry*; Schaefer, H. F., III, Ed.; Plenum Press: New York, 1977; Vol. 3, pp 1−27.
(34) Fukuda, R.; Ehara, M. Effects of perturbation-selection and orbital dependence for the SAC-CI calculations in valence excitations of medium-size molecules. *J. Comput. Chem.* **2014**, *35*, 2163−2176.
(35) Nakatsuji, H.; Hirao, K. Cluster expansion of the wave function. Electron correlation in singlet and triplet excited states, ionized states, and electron attached states by SAC and SAC-CI theories. *Int. J. Quantum Chem.* **1981**, *20*, 1301−1313.
(36) Fukuda, R.; Nakatsuji, H. Formulation and implementation of direct algorithm for the symmetry adapted cluster and symmetry adapted cluster-configuration interaction method. *J. Chem. Phys.* **2008**, *128*, 094105.
(37) Frisch, M. J.; Trucks, G. W.; Schlegel, H. B.; Scuseria, G. E.; Robb, M. A.; Cheeseman, J. R.; Scalmani, G.; Barone, V.; Mennucci, B.; Petersson, G. A.; Nakatsuji, H.; Caricato, M.; Li, X.; Hratchian, H. P.; Izmaylov, A. F.; Bloino, J.; Zheng, G.; Sonnenberg, J. L.; Hada, M.; Ehara, M.; Toyota, K.; Fukuda, R.; Hasegawa, J.; Ishida, M.; Nakajima, T.; Honda, Y.; Kitao, O.; Nakai, H.; Vreven, T.; Montgomery, J. A., Jr.; Peralta, J. E.; Ogliaro, F.; Bearpark, M.; Heyd, J. J.; Brothers, E.; Kudin, K. N.; Staroverov, V. N.; Kobayashi, R.; Normand, J.; Raghavachari, K.; Rendell, A.; Burant, J. C.; Iyengar, S. S.; Tomasi, J.; Cossi, M.; Rega, N.; Millam, M. J.; Klene, M.; Knox, J. E.; Cross, J. B.; Bakken, V.; Adamo, C.; Jaramillo, J.; Gomperts, R.; Stratmann, R. E.; Yazyev, O.; Austin, A. J.; Cammi, R.; Pomelli, C.; Ochterski, J. W.; Martin, R. L.; Morokuma, K.; Zakrzewski, V. G.; Voth, G. A.; Salvador, P.; Dannenberg, J. J.; Dapprich, S.; Daniels, A. D.; Farkas, Ö.; Foresman, J. B.; Ortiz, J. V.; Cioslowski, J.; Fox, D. J. *Gaussian 09*, revision B.01; Gaussian, Inc.: Wallingford, CT, 2010.
(38) Bondi, A. van der Waals volumes and radii. *J. Phys. Chem.* **1964**, *68*, 441−451.
(39) Fukuda, R.; Ehara, M.; Nakatsuji, H.; Cammi, R. Non-equilibrium solvation for vertical photoemission and photoabsorption processes using the symmetry-adapted cluster-configuration interaction method in the polarizable continuum model. *J. Chem. Phys.* **2011**, *134*, 104109.
(40) Nakatsuji, H.; Kitao, O.; Yonezawa, T. Cluster expansion of the wave function. valence and Rydberg excitations and ionizations of pyrrole, furan, and cyclopentadiene. *J. Chem. Phys.* **1985**, *83*, 723−734.
(41) Serrano-Andrés, L.; Merchán, M.; Nebot-Gil, I.; Roos, B. O.; Fülscher, M. Theoretical study of the electronic spectra of cyclopentadiene, pyrrole, and furan. *J. Am. Chem. Soc.* **1993**, *115*, 6184−6197.
(42) Palmer, M. H.; Walker, I. C.; Ballard, C. C.; Guest, M. F. The electronic states of furan studied by VUV absorption, near-threshold electron energy-loss spectroscopy and ab initio multi-reference configuration interaction calculations. *Chem. Phys.* **1995**, *192*, 111−125.
(43) Palmer, M. H.; Walker, I. C.; Guest, M. F. The electronic states of pyrrole studied by optical (VUV) absorption, near-threshold electron energy-loss (EEL) spectroscopy and ab initio multi-reference configuration interaction calculations. *Chem. Phys.* **1998**, *238*, 179−199.
(44) Nakano, H.; Tsuneda, T.; Hashimoto, T.; Hirao, K. Theoretical study of the excitation spectra of five-membered ring compounds: cyclopentadiene, furan, and pyrrole. *J. Chem. Phys.* **1996**, *104*, 2312−2320.
(45) King, H. E., Jr. Compression of organic crystals. *Physica* **1968**, *139&140B*, 168−173.
(46) Vaidya, S. N.; Kennedy, G. C. Compressibility of 18 molecular organic solids to 45 kbar. *J. Chem. Phys.* **1971**, *55*, 987−992.
(47) Thiéry, M. M.; Besson, J. M.; Bribes, J. L. High pressure solid phases of benzene. II. Calculations of the vibration frequencies and evolution of the bonds in C_6H_6 and C_6D_6 up to 20 GPa. *J. Chem. Phys.* **1992**, *96*, 2633−2654.
(48) Pravica, M.; Shen, Y.; Quine, Z.; Romano, E.; Hartnett, D. High-pressure studies of cyclohexane to 40 GPa. *J. Phys. Chem. B* **2007**, *111*, 4103−4108.
(49) Ooshika, Y. Absorption spectra of dyes in solution. *J. Phys. Soc. Jpn.* **1954**, *9*, 594−602.
(50) Longuet-Higgins, H. C.; Pople, J. A. Electronic spectral shifts of nonpolar molecules in nonpolar solvents. *J. Chem. Phys.* **1957**, *27*, 192−194.

DOI: 10.1021/ct5011517
J. Chem. Theory Comput. 2015, 11, 2063−2076

(51) McRae, E. G. Theory of solvent effects on molecular electronic spectra. Frequency shifts. *J. Phys. Chem.* **1957**, *61*, 562−572.
(52) Renger, T.; Grundkötter, B.; Madjet, M. E.-A.; Müh, F. Theory of solvatochromic shifts in nonpolar solvents reveals a new spectroscopic rule. *Proc. Natl. Acad. Sci. U.S.A.* **2008**, *105*, 13235−13240.
(53) Fukuda, R.; Ehara, M. Mechanisms for solvatochromic shifts of free-base porphine studied with polarizable continuum models and explicit solute-solvent interactions. *J. Chem. Theory Comput.* **2013**, *9*, 470−480.

DOI: 10.1021/ct5011517
J. Chem. Theory Comput. 2015, 11, 2063−2076